A transportable optical lattice clock

Stefan Vogt, Sebastian Häfner, Jacopo Grotti, Silvio Koller, Ali Al-Masoudi, Uwe Sterr and Christian Lisdat

Physikalisch-Technische Bundesanstalt, Bundesallee 100, D-38116 Braunschweig, Germany

E-mail: stefan.vogt@ptb.de

Abstract. We present the experimental setup and first results of PTB's transportable ^{87}Sr clock. It consists of a physics package, several compact laser breadboards, and a transportable high finesse cavity for the clock laser. A comparison of the transportable system with our stationary optical lattice clock yields an instability of $2.2 \times 10^{-15}\,\sqrt{\mathrm{s}/\tau}$ for the transportable clock. The current fractional uncertainty of 1×10^{-15} is still limited by the not yet fully evaluated light shift from the free running optical lattice laser operated near the magic wavelength. We are currently improving our transportable system to reach an uncertainty at or below the 10^{-17} level, which will finaly be limited by the uncertainty in blackbody radiation shift correction.

1. Introduction

The performance of optical lattice clocks is now exceeding the Cs clock performance by two orders of magnitude in accuracy and stability. The best lattice clocks reach an uncertainty in the low 10^{-18} range [1, 2] and achieve instabilities of below $2 \times 10^{-16}\sqrt{\mathrm{s}/\tau}$ [3]. This excellent performance offers new prospects for both fundamental science and applications that include the search for variations of fundamental constants, tests of general relativity on a higher level of accuracy, and relativistic geodesy. However, optical clocks that show a fractional instability of 10^{-15} or even 10^{-16} at one second cannot efficiently be compared by the traditional radio-frequency methods that are at best limited at 10^{-13} at one second. In order to exploit the full potential of optical clocks for these scientific applications, new methods for frequency comparisons beyond the current limitations of radio-frequency comparisons have to be developed. Therefore transportable frequency standards or stabilized optical fiber links are necessary. In addition, transportable optical frequency standards in combination with optical fiber links allow for relativistic geodesy (height measurement) [4, 5] at the centimetre level between far-separated points. This method to determine the geopotential is complementary to the state-of-the-art methods of geodesy, since it directly measures differences in the local gravitational potential, while established methods use leveling together with local measurements of the earth acceleration (the spatial derivative of the potential) or a combination of a detailed gravity model and GNSS satellite data. Therefore relativistic geodesy will eventually provide a useful verification and even improvement of geodetic models.

In this paper we describe an optical lattice clock setup based on neutral strontium atoms. The experimental setup is made robust and compact to allow for a transportation to another laboratory or even a remote location using an air-conditioned trailer. The setup was not optimized for extreme power efficiency or small volume but to provide ultimately an optical

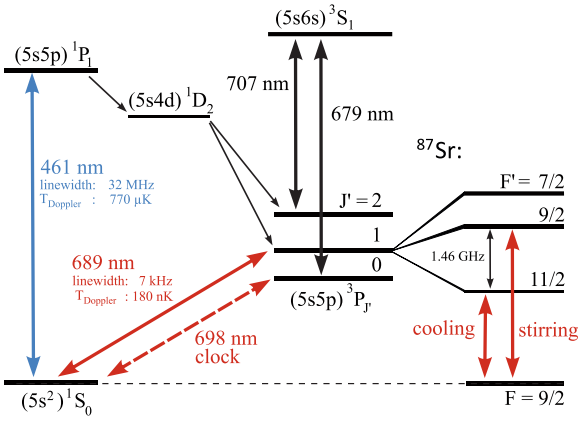

Figure 1. Partial level scheme of strontium. The lattice laser is operating at the Stark-shift-cancellation wavelength near 813 nm. (color online)

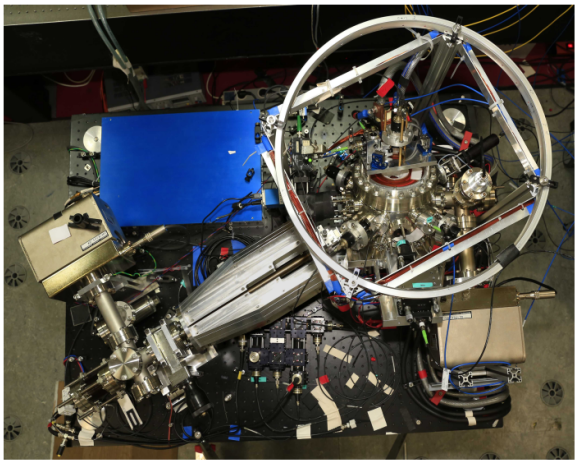

Figure 2. Top view of the physics package. The dimensions of the setup are 1200 mm × 900 mm. (color online)

lattice clock with metrologically competitive characteristics, i.e. uncertainties below 10^{-17} after 10^4 seconds of averaging.

First measurements with the transportable setup have been performed including a comparison with the stationary strontium clock at PTB [6, 3]. The current uncertainty budget has been evaluated leading to an uncertainty of 1.3×10^{-15}. We show that with the completion of the setup that is currently underway, the uncertainty of the system will be improved even below 10^{-17}.

2. Experimental setup

2.1. Laser Modules

For laser cooling of neutral ^{87}Sr atoms, trapping in an optical lattice, and interrogation of the 698 nm $^1S_0$–$^3P_0$ clock transition in total lasers at six different wavelengths are required (see Fig. 1). The lasers are based on commercial extended cavity diode lasers (ECDLs). For atom preparation, a two-stage Magneto-Optical Trap (MOT) sequence is used. In the first stage the 461 nm $^1S_0$–$^1P_1$ transition in the singlet system is used for Zeeman slowing and to efficiently trap the atoms in a MOT. In this stage two repump lasers (679 nm and 707 nm) are used to depopulate the long lived dark $^3P_2$ state, that is populated by a decay channel from the $^1P_1$ state. In the second MOT stage operating on the narrow intercombination line ($^1S_0$–$^3P_1$, 689 nm) the atoms are further cooled down to the μK level.

The lasers are integrated on breadboards that are connected via polarization-maintaining fibers to the physics package. Laser distribution, frequency shifting and switching are done on these compact aluminum breadboards (size: 450 mm × 300 mm) with half inch optics, acousto-optical modulators (AOMs) and mechanical shutters to prevent ac Stark frequency shifts from residual cooling light during clock interrogation. The 461 nm blue light is generated by second-harmonic generation in a resonant doubling cavity.

For second-stage cooling of ^{87}Sr, we use two lasers at 689 nm, called cooling- and stirring laser, which address the 1.46 GHz separated hyperfine transitions $^1S_0$–$^3P_1$, $F = 9/2 - F' = 11/2$ and $F = 9/2 - F' = 9/2$ [7]. The power requirements of about 10 mW per laser can be met with an ECDL without need of an additional injection-locked laser diode. The lattice light is provided by a commercial tapered amplifier (TA) system with an output power of up to 2 W.

For frequency stabilization the lasers are locked to individual 10-cm-long ultra low expansion glas (ULE) cavities. For the 461-nm cooling laser a cavity housed in a simple vacuum chamber with one passive heat shield is sufficient. The temperature of the vacuum chamber is stabilized by thermoelectric coolers (TEC). Changes of the cavity resonance frequency due to residual temperature fluctuations and day-to-day drifts are negligible compared to the linewidth of the cooling transition of about 32 MHz. Because of the considerably narrower linewidth of the red cooling transition ($\approx$ 7 kHz) more care has been taken to stabilize the temperature of the reference resonator for the second-stage cooling lasers. Here, a two-stage temperature stabilization has been applied that actively controls the outside vacuum chamber as well as a heat shield within the vacuum by TECs. The lattice laser will soon be stabilized to a similar cavity setup, which however had not been finalized for the first clock measurements. The finesse of the resonator for the 689 nm cooling is high ($F = 240\,000$) to relax the requirements on the laser stabilization electronics, while the other two cavities have a finesse of around 1000. The frequency stability of the 689 nm cooling laser is transferred to the stirring laser via a phase lock loop with a frequency offset. We do not stabilize the frequency of the repump lasers, because a frequency modulation of several 100 MHz that has to be applied to cover the hyperfine structure of ^{87}Sr leads to relaxed requirements for the frequency stability of the lasers. If necessary the lasers could be locked to a wavelength meter with an accuracy of 200 MHz in the future.

The clock laser system was previously described [8] while the transportable reference cavity was replaced by an improved design [9]. The resonator consists of a 12 cm long ULE spacer with fused silica mirrors. The resonator is rigidly mounted via a wire-bar mounting system, which is attached to Invar pins that are glued into holes in the spacer. The mounting of the cavity is optimized for low vibration sensitivity by applying all retaining forces only normal to the respective symmetry planes and by a kinematic mount, effectively reducing the degrees of freedom within the mounting structure to avoid overdetermination [10, 11]. The sensitivity of the cavity resonance frequency to accelerations in three orthogonal directions is $\kappa = (0.3, 4.3, 11.6) \times 10^{-10}/\mathrm{g}$. We attribute the relatively high sensitivity along the spacer axis to imperfections in the realization of the mounting. Using an active vibration isolation platform (Table Stable TS-150), the thermal noise floor of the resonator setup of 4×10^{-16} is almost reached for timescales of 1 s up to a few 10 s (Fig. 6), as we could show by comparison to a non-transportable clock laser with an instability of below 1×10^{-16} [12].

2.2. Physics Package

As the frequency shift due to blackbody radiation of the environment is a critical factor in strontium lattice clocks [13, 2], special care has been taken to provide a good temperature homogeneity across the vacuum chamber surrounding the interrogated atoms. This includes an efficient water cooling of the coils that are used to generate the magnetic field for magneto-optical trapping and the design of a Zeeman slower using permanent magnets.

The main part of the physics package is the vacuum chamber, which is mounted on a table with the size of 1200 mm $\times$ 900 mm (see Fig. 2). This chamber is separated into two parts: the oven chamber where strontium atoms are evaporated from an atomic oven at about 480 °C, and the main chamber where laser cooling, trapping and the interrogation are performed. Both parts are connected by a 50 cm long Zeeman slower tube. In between the oven region and the Zeeman slower tube, a 2-mm-diameter pinhole is used to shield the MOT region from the blackbody radiation of the oven. It also enables differential pumping between the oven and the MOT chamber to maintain a pressure ratio of about one order of magnitude during operation of the apparatus. In the oven chamber a rotation shutter is used to fully block the radiation from the hot oven during the clock interrogation. The switching of the shutter with an servo motor outside the vacuum takes less than 35 ms, so that switching during one experimental cycle is possible. The surfaces closest to the atom position are the windows of re-entrant flanges with

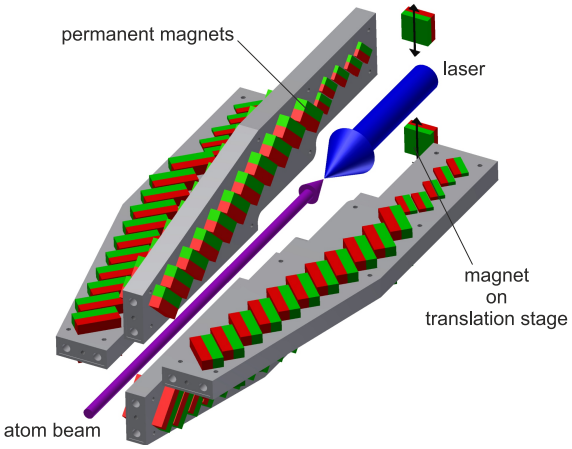

Figure 3. Sketch of the mechanical setup for the Zeeman slower with B-field along the axis. (color online)

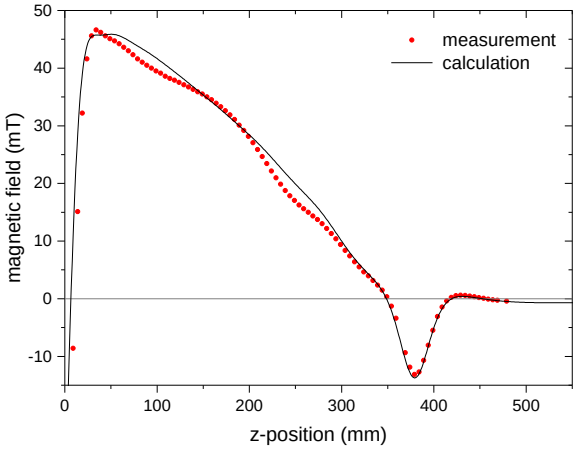

Figure 4. Longitudinal magnetic field component along the slowing axis (z). (color online)

a separation of 54 mm. Those are coated on the inside with a conducting ITO layer to avoid patch charges that would lead to a dc Stark effect. A residual electric charge of 100 mV would lead to a fractional frequency shift in the order of 10^{-19}. Both parts of the chamber are pumped with 40 litres/second ion getter pumps. During operation, the pressure in the main part of the chamber is 2×10^{-9} mbar, leading to a lattice lifetime of about one second. This lifetime is long enough for clock operation with typical interrogation times of about 150 ms limited by the coherence time of the clock laser.

2.3. Zeeman slower with permanent magnets

While direct loading atoms from the background using 2D-MOT – 3D-MOT techniques has been proven to be very useful to cool alkaline atoms, Zeeman slowing [14] is a robust method to provide high flux of slow atoms from elements with low vapor pressure. To avoid the power dissipation and thus heating by the solenoid permanent magnets can be used; an approach that has been chosen by several groups [15, 16, 17, 18] recently.

However, most of these Zeeman slowers produce a magnetic field that is oriented perpendicularly to the atomic beam. The main disadvantage of this transverse field configuration is that only half of the power of the slowing beam has the correct polarization for slowing the atoms – the other half is wasted. The design of a magnet-based Zeeman slower with a magnetic field parallel to the atomic beam is more challenging and more magnetic material has to be used [19]. For this setup we designed and built a Zeeman slower with a longitudinal field, because the ineffective use of blue laser power in the transverse case would be a major drawback especially in a transportable setup.

For our Zeeman slower, we have tried to match the magnetic field of an existing solenoid-based slower, which shows an excellent performance in our stationary strontium clock. The maximum capture velocity of the setup is adapted to an oven temperature of 380 °C to 450 °C.

To get the desired longitudinal field standard sized NdFeB magnet blocks[1] are arranged symmetrically around the beam axis such that the transverse components cancel out (Fig. 3). A ring of four magnets is needed to provide the desired field. The distance of each quadruple of

[1] Two types of magnets are used, remanence B_r = 1.35 T (1.3 T) and dimensions 30 mm × 30 mm × 15 mm (20 mm × 20 mm × 10 mm).

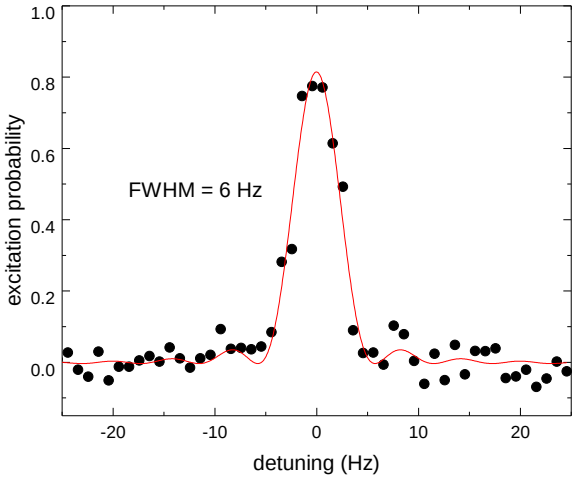

Figure 5. Nearly Fourier-limited linespectrum of the $^1S_0$–$^3P_0$ clock transition in a spin polarized sample of ^{87}Sr atoms interrogated with a probe time of 170 ms. (color online)

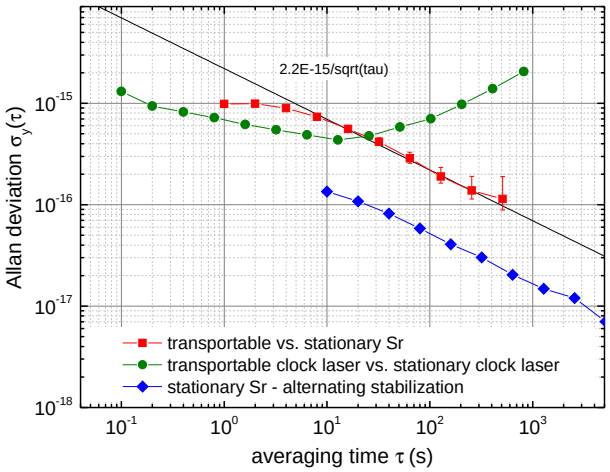

Figure 6. Allan deviation for a 20 minute comparison between stationary and transportable strontium lattice clock (squares). For comparison we show the instability of the reference cavity (circles) [12] and the instability of the stationary strontium clock (diamonds) [3]. (color online)

magnets to the axis can be used for fine tuning of the field near their z-position. An iterative algorithm had to be applied to fit all magnet positions to produce the design field. We have been systematically varying different parameters such as the total number of magnet blocks distributed equidistant along the length of the slower and the size of magnets for each ring. The magnets have been tilted by 45° with respect to the optical axis, to reduce unwanted stray-fields near the MOT. The final design was realized by tightly fitting the magnets into a rigid aluminum holder. With this fixed mount, we were able to get very close to the first (positive) part of the field without further adjustment of the individual magnet blocks as shown in Fig. 4.

To experimentally optimize the field at the output of the Zeeman slower, we firstly adjust the position of the two last magnets that form the part of the magnetic field where the atoms leave the slowing region. These are mounted on translation stages and can be radially moved to tune the magnetic field and hence the minimum velocity of the atoms interacting with the slowing beam, which is a critical part for MOT loading. The second parameter is the detuning of the slowing laser to the atomic resonance. A smaller detuning leads to a reduced capture velocity from the thermal beam, but makes the system more robust against rapid changes of the magnetic field along the slowing axis. Due to such imperfections atoms could otherwise leave the slowing process at a high velocity and would not be captured in the MOT.

We characterized the performance of our slower by measuring the velocity distribution through the Doppler profile on the 461-nm transition of the slowed atomic beam and the loading rate of the MOT. We find that 5×10^8 atoms (^{88}Sr) per second can be captured in the MOT. The velocity distribution shows that atoms can be slowed from about 450 m/s down to 70 m/s without significant loss at intermediate velocities. The loading time needed for regular clock operation with ^{87}Sr is 300 ms, which is similar to the performance of the solenoid Zeeman slower in our stationary experiment.

effect	**correction** (10^{-16})	**uncertainty** (10^{-16})
lattice ac Stark	0	13.0
BBR ac Stark	48.8	0.07
BBR ac Stark oven	0	1.1
2nd order Zeeman	1.2	0.12
line pulling	0	0.07
servo error	0	1.5
ac Stark probe	0	0.05
unstabilized fiber	0	3.0
cold collisions	0	1.0
background gas collisions	0	0.2
total	50.0	13.5

Table 1. Uncertainty budget of the transportable strontium clock. Currently it is dominated by the not yet fully evaluated Stark shift from the free running lattice laser.

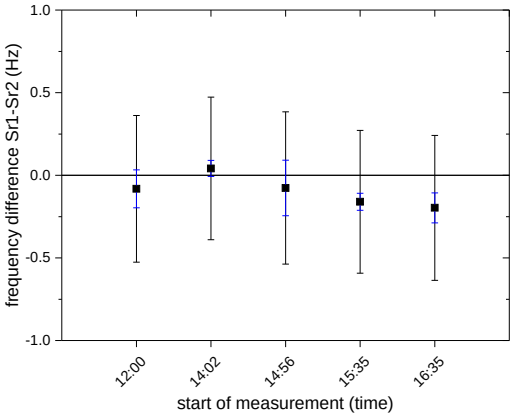

Figure 7. Frequency difference between stationary (Sr1) and transportable (Sr2) strontium clock from typically 1200 s long comparisons. The blue error bars indicate the statistical uncertainty while the black bars indicate the total uncertainty. (color online)

3. Clock comparison and uncertainty budget

We compared the frequency of our transportable clock to our stationary strontium lattice clock [6, 3], while both systems were locked to the clock transition in ^{87}Sr using the average of the two stretched m_F states. For this comparison two completely independent clock lasers were used and the interrogation cycles of the clocks were not synchronized. The stationary clock has shown an estimated instability of $5 \times 10^{-16}\ \sqrt{\mathrm{s}/\tau}$ in an interleaved self comparison (Fig. 6) which is an upper bound for the instability under normal operation. The measured instability of $2.2 \times 10^{-15}\ \sqrt{\mathrm{s}/\tau}$ for the comparison, also shown in Fig. 6, is thus dominated by the performance of the transportable clock. The instability of the transportable clock is limited by the transportable clock laser, which allows us to resolve a 6 Hz Fourier-limited linewidth for the clock transition (Fig. 5). This result was achieved in a fully independent fashion, i.e. without using techniques like correlated interrogation. Therefore this instability can be delivered by the transportable clock in future measurements without relying on the availibility of additional equipment.

The frequencies of the two clocks agree within the uncertainty of the measurement (Fig. 7). The stationary clock has an uncertainty of 3×10^{-17}. This does not contribute significantly to the uncertainty of the measurements. The contributions to the uncertainty of the transportable clock was evaluated in Table 1.

3.1. Lattice light shift

Even though the frequency of the lattice laser was not stabilized during the first measurement campaign, a preliminary uncertainty budget for the transportable clock was evaluated (Fig. 1). The frequency of the lattice laser was monitored via a beatnote with the lattice laser of the stationary strontium system. By comparison with this system, the lattice frequency of the transportable system was known to be near the Stark-shift-cancellation wavelength for ^{87}Sr ($m_F = 9/2$). It is necessary to measure the exact Stark-shift cancellation wavelength for each clock separately, because parameters like the angle between magnetic field and polarization or spurious spectral components of the lattice laser influence the the Stark-shift cancellation

wavelength significantly. During the time we were running a comparison measurement (about 20 minutes), the lattice laser frequency was stable to within 50 MHz, corresponding to an uncertainty contribution of 2.3×10^{-16}. With this lattice laser frequency we tried to determine the magic wavelength by operating the clock at 5 lattice depths between about 70 E_{recoil} and 140 E_{recoil}. However, because of inconsistencies in the data that might be due to the application of a TA laser system for the optical lattice [20], we can only obtain a frequency uncertainty due to the unknown Stark-shift cancellation wavelength of 1.3×10^{-15}.

It is known that spurious spectral components in the lattice lasers emission can compromise the measurement of the Stark-shift cancellation wavelength [20]. Thus we use a volume Bragg grating with a linewidth of 0.1 nm for spectral filtering and a short optical fiber between grating and AOM for spatial mode filtering and spatial superposition of remaining spectral components. Further investigations are urgently required to decide whether this setup will be able to support a more precise determination and cancellation of the lattice light shift.

3.2. Blackbody radiation shift

The blackbody radiation shift has contributions from two sources. One stems from the blackbody radiation of the hot (480 °C) oven. This radiation can be easily blocked by the mechanical shutter in the oven chamber. With the shutter this relatively high uncertainty contribution of 1.1×10^{-16} will be reduced to below the 10^{-18} level. The second part of the blackbody radiation shift is coming from incomplete knowledge of the characteristic temperature of the vacuum chamber. We measure the temperature of the chamber with eight Pt100 sensors placed at critical places around the chamber. During clock operation we find a temperature difference of 250 mK between the hottest and the coldest point. Taking this difference as the width of are rectangular probability distribution for the true representative temperature [6], we obtain an uncertainty contribution of 7×10^{-18}, where the uncertainty of the shift coefficient does not play a significant role [13, 1].

3.3. Other effects

We have performed a preliminary investigation of the other frequency shifting effects that could be relevant at an uncertainty level of 10^{-16} (as shown in Tab. 1). As the measurement uncertainty was limited by the residual lattice ac Stark shift, no special care was taken to minimize these effects. This will be the next step after the characterization of the lattice light shifts. However, even without special optimization most of the effects are at the low 10^{-16} level and can be lowered by one order of magnitude or even more, as has been shown in our stationary lattice clock experiment [6], which employs identical techniques in all critical parts. At the moment the largest uncertainty contributions are due to an unstabilized part of the optical path, which is connecting the clock laser and the physics package, and the servo error, from the non-optimized gain settings for the stabilization to the atomic resonance. We give a comparatively large number for the optical path-length stabilization, because we have observed frequency shifts of this size due to AOM heating in the past. Furthermore, the frequency shift due to cold collisions was only calculated from an estimated density, based on a roughly known atom number. This results in a very conservative uncertainty for the collisional shift of 1×10^{-16}.

4. Summary and Conclusion

In this paper we have presented the first evaluation of an autonomous transportable optical clock based on fermionic strontium using a fully transportable clock laser. The clock showed an excellent instability of $2.2 \times 10^{-15}\ \sqrt{\mathrm{s}/\tau}$ in a comparison with a more stable laboratory system, and an agreement between the two clocks within the uncertainty of the transportable clock. This uncertainty was limited to 1.3×10^{-15} due to the not yet fully evaluated lattice light shift. With the modification that are mentioned in the text, we expect that the uncertainty can be further

improved the near future. Especially the proximity of a well evaluated strontium lattice clock will simplify the evaluation of the transportable clock and make it well suited for measurements in relativistic geodesy that are planned in the near future. In a few years from now, when optical fiber links will be available between various metrology labs throughout Europe, the transportable clock can enable relativistic geodesy with high accuracy along the links.

5. Acknowledgments

This work was performed within the framework of the Centre of Quantum Engineering and Space-Time Research (QUEST). We acknowledge funding from the German Research Foundation DFG within the collaborative research center CRC 1128 geo-Q and research training group RTG 1729, from the Marie-Curie Action ITN "FACT" and from the ITOC and QESOCAS projects in the European Metrology Research Programme EMRP. The EMRP is jointly funded by the EMRP participating countries within EURAMET and the European Union.

References

[1] Nicholson T L *et al* 2015 Nature Com. **6** 6896
[2] Ushijima I *et al* 2015 Nature Photonics **9** 185
[3] Al-Masoudi A *et al* 2015 Phys. Rev. A **92** 063814
[4] Bjerhammar A *et al* 1985 Bulletin Géodésique **59** 207
[5] Verhaar B J *et al* 1987 Phys. Rev. A **35** 3825
[6] Falke S *et al* 2014 New J. Phys. **16** 073023
[7] Mukaiyama T *et al* 2003 Phys. Rev. Lett. **90** 113002
[8] Vogt S *et al* 2011 Appl. Phys. B **104** 741
[9] Häfner S 2015 Ultrastabile Lasersysteme für Weltraum und Boden-Anwendungen Ph.D. thesis Leibniz Universität Hannover (Online: http://edok01.tib.uni-hannover.de/edoks/e01dh16/84568972X.pdf)
[10] Sterr U 2011, Frequenzstabilisierungsvorrichtung German patent DE 10 2011 015 489
[11] Chen Q F *et al* 2014 Rev. Sci. Instrum. **85** 113107
[12] Häfner S *et al* 2015 Opt. Lett. **40** 2112
[13] Middelmann T *et al* 2012 **109** 263004
[14] Phillips W D and Metcalf H 1982 Phys. Rev. Lett. **48**, 596
[15] Ovchinnikov Y B 2007 Opt. Commun. **276** 261
[16] Ovchinnikov Y B 2008 Eur. Phys. J. Special Topics **163** 95
[17] Chen Z *et al* 2011 Phys. Rev. Lett. **106** 133601
[18] Hill I R *et al* 2012 in *European Frequency and Time Forum (EFTF)* (IEEE) pp. 545–549.
[19] Ovchinnikov Y B 2011 Opt. Commun. **285** 1175
[20] Le Targat R *et al* 2012 *European Frequency and Time Forum (EFTF)* (IEEE) Contribution to European Frequency and Time Forum 2012, Gothenburg, Sweden